

QUANTIFYING THE NGVLA'S CONTRIBUTION TO EXO-SPACE WEATHER: RESULTS OF A COMMUNITY STUDIES REPORT *NEXT GENERATION VLA MEMO # 31*

RACHEL A. OSTEN¹
Space Telescope Science Institute

MICHAEL K. CROSLLEY
Physics & Astronomy Dept., Johns Hopkins University, Baltimore, MD
Draft version November 13, 2017

ABSTRACT

A forward-looking facility such as the next generation Very Large Array (ngVLA) requires forward-looking science. The ngVLA will enable stellar wind detections or robust constraints on upper limits sufficient to bridge the gap between current radio upper limits on cool stellar mass loss and current indirect estimates of stellar mass loss from astrospheric measurements. This will aid in understanding the interplay between the rotational spindown of stars and wind mass loss rates, important for an understanding not just of stellar astrophysics but the impact on planet formation and planetary dynamos. Radio observations are currently the only way to explore accelerated particles in cool stellar environments. The upgraded sensitivity of the ngVLA will enable the detection and characterization of essentially all classes of radio-active cool stars in the galaxy. This will open up new fields of study and contribute to the understanding of the stellar contribution to exo-space weather, especially with the emphasis on sensitivity above a frequency of about 10 GHz, where the transition to optically thin gyrosynchrotron emission occurs. These topics connect and extend the key science topics in the cradle of life, in an area which there is both high academic as well as popular interest, and which is expected to continue into the next several decades.

1. INTRODUCTION

With the announcement by the Kepler mission of more than two thousand confirmed transiting exoplanets, population statistics suggesting that a transiting exoplanet in the habitable zone of its star likely resides within 5 pc (Dressing & Charbonneau 2013), and recent confirmation via radial velocity techniques of a planet in the habitable zone of our nearest star (Anglada-Escudé et al. 2016), astronomy is firmly in the age of exoplanets. This is an area which grabs the public's attention as well as unites professional astronomers, planetary scientists, and astrobiologists, in the search for life. Ground- (MEarth project) and space-based (TESS, PLATO) projects have as their primary goal the discovery of even more, closer transiting exoplanets, and large ground- and space-based projects like the James Webb Space Telescope and giant segmented mirror telescopes (E-ELT, TMT, GSMT) will characterize their atmospheres. Characterizing the atmospheres and environments of potentially habitable exoplanets will be a major focus of the astronomical community in the next ten to twenty years. During that time, we can expect that the phase space for exoplanet demographics will be fleshed out, with major inroads into understanding the interrelationship between planet properties and stellar properties. There will be many potentially habitable worlds, and one major question will be how to move beyond that potentiality into a more informed as-

essment of the likelihood of seeing an *inhabited* world.

Stellar activity is known to be able to create false positive signatures in biomarkers (Tian et al. 2014). Planetary habitability is a multi-faceted issue and depends not just on the planetary parameters, but is strongly influenced by the environment set by the host star. The star can influence the planetary environment through radiation and particles. Stellar flaring and associated coronal mass ejections, a steady stellar wind, and star-planet magnetospheric interactions are all important factors in the space weather environments of these exoplanets. Radio emission is the only wavelength regime capable of placing direct constraints on the particle environment that stars produce, and adds significant information on the steady mass loss of nearby stars.

2. MASS LOSS ON THE LOWER HALF OF THE MAIN SEQUENCE

Stellar winds affect the migration and/or evaporation of exoplanets (Lovelace et al. 2008), and are important not only for understanding stellar rotational evolution, but it also their influence on planetary dynamos (Heyner et al. 2012). At present only indirect measures of cool stellar mass loss inform these topics. Mass loss in the cool half of the HR diagram, along/near the main sequence, has been notoriously difficult to detect directly, due in part to the much lower values of mass loss here compared to other stellar environments (\dot{M} of 2×10^{-14} solar masses per year for the Sun). Detection of Lyman α astrospheric absorption (Wood et al. 2004) does not detect the wind directly, but rather

osten@stsci.edu

¹ Also at Center for Astrophysical Sciences, Johns Hopkins University, Baltimore, MD 21218

the bow shock created when the wind interacts with the local interstellar medium. This can only be done with high-resolution ultraviolet spectrographs in space; currently the Space Telescope Imaging Spectrograph on the Hubble Space Telescope, installed in 1997, is the only instrument capable of making such measurements. Non-detections of this feature do not provide upper limits to the stellar mass loss.

Cool stellar mass loss is characterized by an ionized stellar wind, whose radio flux can have a $\nu^{0.6}$ or $\nu^{-0.1}$ dependence if in the optically thick or thin regime, respectively. A direct measurement of stellar mass loss through its radio signature would be a significant leap forward not only for understanding the plasma physics of the stars themselves, but also for understanding what kind of environment those stars create. Previous attempts at a direct detection of cool stellar mass loss via radio emission have led to upper limits typically three to four orders of magnitude higher than the Sun's present-day mass loss, while indirect methods find evidence for mass loss rates comparable to or slightly higher than the Sun's present day mass loss rate (up to ~ 80 times solar \dot{M} .)

Initial work assessing the feasibility of the ngVLA's ability to detect directly the stellar winds of nearby cool, main sequence stars was done as part of the Bower et al. (2015) report of ngVLA Working Group 4. This brief work used analytic formulae in Drake et al. (1987), based on the expected optically thick and thin radio emission from an ionized stellar wind presented in Wright & Barlow (1975), and Panagia & Felli (1975); optically thick emission from an ionized stellar wind is expressed as

$$S_\nu = 1.6 \times 10^{11} \left(\frac{\dot{M}}{v_w} \right)^{1.33} \frac{\nu_5^{0.6} T_4^{0.1}}{d_{kpc}^2} \quad (1)$$

where S_ν is the predicted radio flux in mJy per beam, \dot{M} is the mass loss rate in solar masses per year, v_w is the velocity of the stellar wind, ν_5 is the frequency normalized to 5 GHz, T_4 indicates the temperature of the solar wind in units of 10^4 K, and d_{kpc} is the distance in kpc. As winds from late-type stars are presumed to originate in the open field lines of the outer corona, a coronal wind temperature of 10^6 or $T_4=100$ is used. We expand on these calculations to different frequencies in the expected ngVLA range, and incorporate demographics of the nearest stars using catalogues of nearby stars. We use the recent continuum sensitivities quoted for the ngVLA at a variety of frequencies as posted at <http://science.nrao.edu/futures/ngvla/concepts>, extended for a 12 hour integration. The stellar escape velocity is ~ 600 km s $^{-1}$ for main sequence solar-like stars and cooler, and the minimum constrainable mass loss rate for this velocity is quoted in this memo. However, we note that recent results from studies of exoplanets (Vidotto et al. 2015 and others) have found evidence for hot Jupiters embedded in slower stellar winds than would be expected based on solar scalings, with expectations of a denser stellar wind than experienced by solar system planets. With this in mind, we explore a range of assumed wind speeds, from 100 to 1200 km s $^{-1}$.

2.1. Increasing the Look-back Time for Studying the Young Sun

Table 1 lists nearby commonly used solar analogs within 15 pc from the Sun, and their ages. Results from high spectral resolution UV data of nearby stars where astrospheric absorption is seen suggest that there is a power-law relationship between inferred mass loss and surface X-ray flux, with a limit in surface X-ray flux of about 10^6 erg cm $^{-2}$ s $^{-1}$, above which no or significantly reduced mass loss is inferred. This limits the ability to constrain the mass-loss history of the Sun, using analogues. In particular, the lack of detection of this feature does not provide any quantitative constraints on the mass-loss of that star. Based on this work, the most active stars appear not to have strong winds; there is evidence via astrospheric detection towards the nearby young solar analog π^1 UMa (Wood et al. 2014), with age estimates between 300 and 500 million years, of a weak wind from the young Sun.

There is tension between the results returned from the astrospheric detection method and the mass loss expected from stellar rotational evolution models. Stars are expected to lose angular momentum in a wind as their rotation decreases with time; the rate of rotation period decrease can be determined from distributions of rotation periods in clusters of known ages, while MHD wind models are required to interpret the implied mass loss rates which should accompany this. Johnstone et al. (2015) performed such calculations, suggesting that the stellar mass-loss rate can be parameterized as

$$\dot{M}_* \propto R_* \Omega_*^{1.33} M_*^{-3.36} \quad (2)$$

The results suggest that the Sun at young ages should have had a mass loss rate roughly an order of magnitude higher than it does today. Fichtinger et al. (2017) presented recent results obtained from the JVLA and ALMA for a sample of nearby stars. Results are shown in Figure 1. They expanded upon the earlier spherically symmetric wind models, and showed that a conical opening angle for the wind can reduce the mass loss rate implied from a given radio flux density by about a factor of two compared to the spherically symmetric case. Their upper limits for implied mass loss are still two to three orders of magnitude above the levels of mass loss implied from the rotational evolution models, which themselves are about an order of magnitude above the mass loss rate implied by the detection of astrospheric absorption from the nearby solar analogue π^1 UMa. Results from the ngVLA will be able to make a significant leap in understanding the mass loss history of the Sun through its two order of magnitude improvement over what can be achieved at present with the JVLA. In addition, non-detections provide quantitative constraints on the mass loss rate, a marked difference from the astrospheric absorption method.

2.2. M Dwarfs in the Solar Neighborhood

After initial skepticism about the possibility of M dwarfs hosting exoplanets, attention is fully fixed on these cool dim stars. M dwarfs are the most common type of star in our galaxy, and recent results have shown a high occurrence rate of planets around M dwarfs.

TABLE 1
COMMONLY USED SOLAR ANALOGS AND POTENTIAL ngVLA
MASS-LOSS CONSTRAINTS

Name	Age (MY)	Distance (pc)	\dot{M} constraint ^{1,2} (\dot{M}_\odot)
EK Dra	100	34	425
χ^1 Ori	300	8.7	55
π^1 UMa	500	14.3	116
κ^1 Cet	650	9.2	60

¹ Using ngVLA sensitivity at 17 GHz, extrapolated for a 12 hour integration

² For $\dot{M}_\odot = 2 \times 10^{-14} M_\odot \text{ yr}^{-1}$ and wind speed equal to escape speed

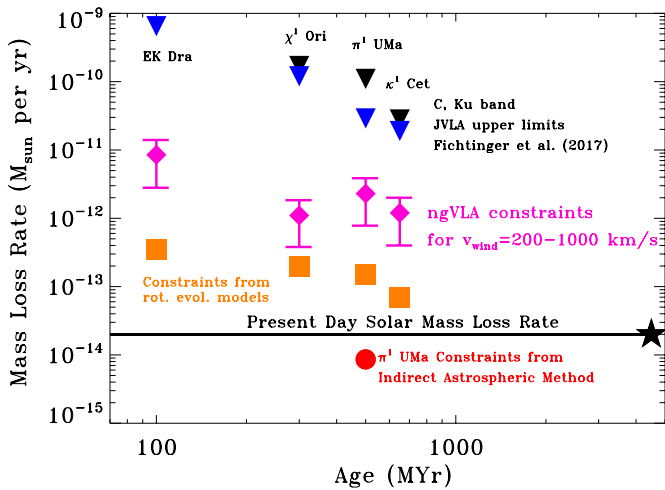


FIG. 1.— Summary of current mass loss constraints for nearby solar analogs, along with prospects achievable with the ngVLA. Black and blue triangles indicate upper limits from C and Ka bands obtained with the JVLA (Fichtinger et al. 2017) for spherically symmetric winds; orange squares show mass loss constraints from the rotational evolution models of Johnstone et al. (2015); and red circle shows detection from the indirect method of inferring mass loss via astrophysical absorption (Wood et al. 2014). Magenta diamonds and error bars display the grasp of the ngVLA, for wind velocities spanning 200–1000 km s⁻¹. The present-day solar mass loss rate is $2 \times 10^{-14} M_\odot \text{ yr}^{-1}$.

This makes planets around M dwarfs one of most common modes of planet formation in our galaxy. The magnetic activity of M dwarfs can have significant influence on the chemistry and dynamics of these planets’ atmospheres due to the planets’ close proximity to the star, and these effects may be observable with JWST (Venot et al. 2016). Recent results (Garaffo et al. 2016, 2017) have shown that the stellar magnetosphere influences the inner edge of the traditional habitable zone. In the case of the iconic TRAPPIST-1 system of seven planets, magnetospheric models suggest that all but two of these planets would have orbits crossing the Alfvén surface and thus would experience severe space weather. Thus consideration of the steady stellar wind as well as time-varying flares and coronal mass ejections from M dwarfs are vital components to understanding the complex intertwining that may or

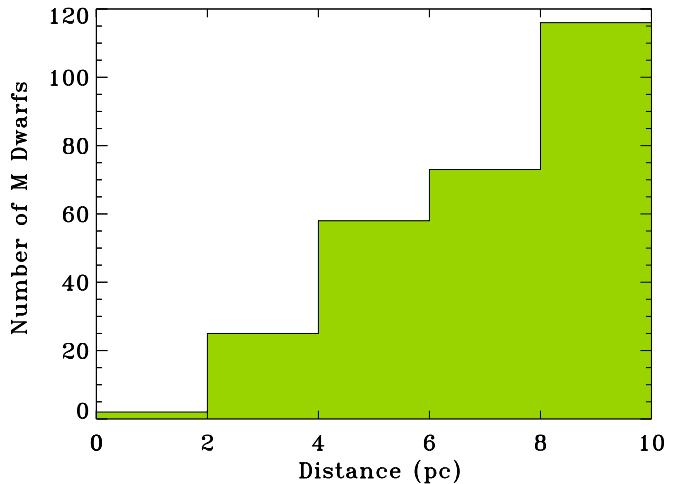


FIG. 2.— Number of M dwarfs as a function of distance, from the REsearch Consortium of Nearby Stars (RECONS). There are more than about 270 M dwarfs within 10 pc; several of these are known to host exoplanets and by the time of the late 2020s all of these will have been surveyed for close-in exoplanets. An important constraint for further characterization of these exoplanets will be the extent to which the star makes its proximate environment helpful or harmful for habitability.

may not turn a potentially habitable planet into an inhabited planet. Current studies suggest that there are about 270 M dwarfs within 10 pc (Figure 2). Several of these are already known to host exoplanets; by the time that the ngVLA is operational, at the end of the 2020s, all of these will have been surveyed for both close-in exoplanets (via the transit method), and those in more distant orbits (by coronagraphy). Radio observations to constrain the mass loss from a steady stellar wind will be crucial measurements to add to the mix to understand the impact the star may have on exoplanet companions.

Very little is known observationally about the mass-loss of nearby M dwarfs. The nearby, magnetically active M dwarf EV Lac is one exception, having had an astrophysical detections from Lyman α absorption. The inference is for a mass loss rate of only 0.7 times the solar mass loss rate, after correcting the results of Wood et al. (2004) for the much smaller surface area of EV Lac. Wargelin & Drake (2001) presented a different method for detecting stellar winds, which makes use of an X-ray charge exchange halo which should exist between the highly charged ions in the stellar wind and the surrounding ISM. This method is promising; they were able to provide an upper limit to the mass loss rate of Proxima at $3 \times 10^{-13} M_\odot \text{ yr}^{-1}$, with approximately a factor of three uncertainty in their model. This requires the use of a space-based X-ray emission with sufficient sensitivity and spatial resolution to resolve this emission from the stellar coronal emission, expected to be thousands of times stronger (the spatial resolution is required to discern this signature in the wings of the coronal PSF). This may be a complementary approach to the detection of radio emission of an ionized stellar

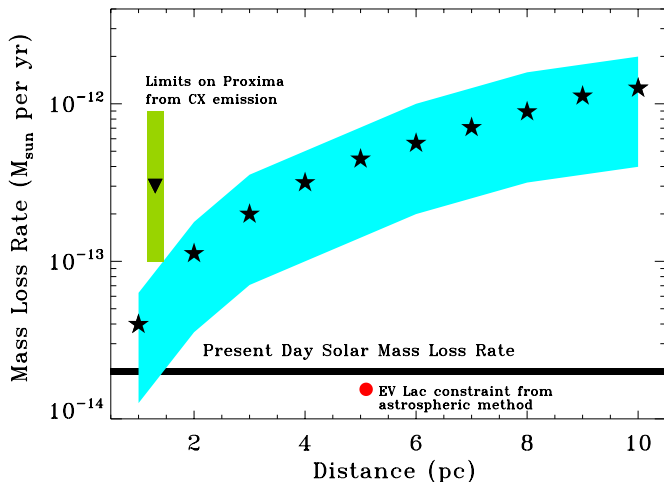


FIG. 3.— Regions of stellar mass loss rate which can be constrained by a 12 hour ngVLA integration for studies of radio emission from an ionized stellar wind, for M dwarfs at a range of distances from 1-10 pc. Stars indicate expected amount of optically thick emission at 28 GHz from a spherically symmetric wind with wind velocity equal to the escape velocity, and cyan shaded region gives area encompassed by a range of assumed wind velocities, from 200 - 1000 km^{-1} . Current observational limits on M dwarf wind mass loss are indicated at the distance of the objects: the green triangle indicates the upper limit for Proxima based on limits from charge exchange emission (Wargelin & Drake 2001), along with the uncertainty in their model. The stellar wind mass loss rate implied by the detection of Lyman α astropheric absorption towards the M dwarf EV Lac at 5.1 pc is also indicated.

wind, possible with the Lynx mission concept under study by NASA with 50 times Chandra’s sensitivity and Chandra-like angular resolution. Because of the angular resolution requirement, it is most competitive for stars within about 5 pc.

The method of detecting radio emission from nearby M dwarfs will be an important contributor to understanding how the wind environment of nearby M dwarfs contributes to the habitability of orbiting exoplanets. Figure 3 shows the sensitivity of the ngVLA to detecting radio emission from an ionized stellar wind for M dwarfs within 10 pc, using similar methods as described in the above section for the mass loss history of the Sun. The green triangle depicts the constraint on mass loss rate for the nearest M dwarf, Proxima, described above, along with the estimated uncertainty in the model. The red circle shows the mass loss rate in solar masses per year for the nearby M dwarf EV Lac, as obtained from the detection of astropheric absorption.

2.3. Interpretation of Radio Emission

While measurements of radio emission from point sources are easy to undertake, their interpretation is complicated. The calculations in the above subsections have been performed under the assumption of optically thick emission, in which case the emission increases as $\nu^{0.6}$. The commonly observed gyrosynchrotron emission from radio active stars typically has a peak frequency near 10 GHz, with flat or slightly negative spectrum at higher frequencies. Indeed, the upper limits returned by Fichtinger et al. (2017) were obtained after careful removal of observed variable emis-

sion attributed to gyrosynchrotron emission. The peak frequency is a function of activity, so observations at higher frequencies are necessary to separate any wind emission from these other sources. At even higher frequencies such as those probed by ALMA, stellar chromospheric emission is detected. Thus the region between 10 and 100 GHz is ideal for searching for wind emission from nearby stars.

The stellar wind must be optically thin to nonthermal radio emission originating closer to the stellar surface. The time-averaged mass-loss from coronal mass ejections, considered a component of a stellar wind, can not be higher than a steady spherically symmetric stellar wind. Both Drake et al. (2013) and Osten & Wolk (2015) have argued for a high flare-associated transient mass loss from active stars; for the young solar analog EK Dra flare-associated CME-induced mass-loss rate of $4 \times 10^{-11} M_{\odot} \text{yr}^{-1}$. The mass loss rate of M dwarfs is expected to vary widely as a function of magnetic activity, with flare-associated mass loss rates of 10^{-12} and $10^{-11} M_{\odot} \text{yr}^{-1}$ for the active M dwarfs AD Leo and EV Lac, respectively, both at distances of about 5 pc. Constraints from ngVLA measurements would be below both of these numbers, and would provide a robust constraint on the breakdown of flare-CME connections, as implied in Crosley et al. (2017). Instrument requirements are a large enough bandwidth to disentangle different contributions to the spectral energy distribution and mitigate variability expected to dominate in the lower frequency bands, and circular polarization for additional constraints on ruling out nonthermal emission.

3. PARTICLES AND FIELDS: CONTRIBUTION TO EXO-SPACE WEATHER

Habitability studies are interested in the flux of accelerated particles directed outward from the stellar surface; the most energetic ones are the most impactful to an exoplanetary atmosphere. Studying the population of accelerated particles near the stellar surface can provide details of the particle spectrum. Comparison to well-studied solar events enables systematics with respect to scalings or extrapolations used for stellar space weather calculations to be investigated. Segura et al. (2010) investigated the impact on the ozone layer of a superflare from an M dwarf. The energetic particles can deplete the ozone layer of a planet in the habitable zone of an Earthlike planet around an M dwarf experiencing a superflare.

Radio observations provide the clearest signature of accelerated particles and shocks in stars arising from transient magnetic reconnection, and provide more realistic constraints on these factors than scaling by solar values (Osten & Wolk 2017). Optically thin gyrosynchrotron emission constrains the index of the accelerated particles, and also enables a constraint on magnetic field strengths in the radio-emitting source (Smith et al. 2005, Osten et al. 2016). The peak frequency is about 10 GHz, so observations at higher frequencies are necessary to disentangle optical depth effects from the interpretation.

3.1. Radio-Active Cool Stars

Variable stellar radio emission in the cool half of the HR diagram is more typical than steady flux levels, at

least at microwave frequencies. This is a consequence of the dominance of emission from accelerated particles, and an indicator of the nonsteady levels of particle acceleration, varying as a function of position on the stellar disk and time. While previous studies estimating the contribution of stellar magnetic reconnection flaring from different types of active stars have used average or “typical” flux densities, the existence of extreme levels of variability (up to 1-2 orders of magnitude) make this approach susceptible to biases. The timescales for stellar flares can vary from milliseconds, in the case of some highly circularly polarized radio bursts (Osten & Bastian 2006, 2008), to minutes to many hours or days for the most dramatic examples (Richards et al. 2003).

We examined objects characteristic of their class for several types of radio-active cool stars illustrating a large amount of variability. This included Algol, RS CVn, and BY Dra active binaries, and nearby magnetically active mid-M and late-M dwarf stars. We used a radio luminosity distribution which gives the range of radio emission expected to be observed for each type of object, under the assumption that the flux variation seen in one object is typical of the class. Figure 4 shows this time-domain information recast as a cumulative probability distribution for each object. The time-domain information for Algol, HR 1099, σ^2 CrB, and UX Ari is taken from multi-year monitoring with the Green Bank Interferometer (Richards et al. 2003). The M dwarf distribution comes from extensive 8 GHz light curves of the nearby M dwarf EV Lac (Osten et al. 2005, Osten et al. in prep.), while the ultracool dwarf LP349-25 was used for the distribution of radio luminosities for ultracool dwarfs (Ngoc et al. 2007, Osten et al. 2009). For young stellar objects, the radio luminosity distribution was obtained from the 556 sources detected in the deep centimeter wavelength catalog of the Orion Nebula Cluster (Forbrich et al. 2016). For this sample, objects with negative spectral index were removed as potential contaminating extragalactic sources, and the distribution of radio luminosities for the remaining 478 sources was computed.

We used demographic information and space densities (listed in Table 2) to come up with a likelihood of observing a given radio luminosity level for types of stars at a given distance. This is more probabilistic and represents reality better than taking the largest radio luminosity of a given type, assuming that that is characteristic level of radio emission, and projecting that to find the farthest distance to which the system is sensible, to arrive at source numbers. An rms for given frequency and integration time determines the distance to which an observation is sensitive, for a source of a particular radio luminosity,

$$L_R = F_{3\sigma} 4\pi d_{\text{sens}}^2 \quad (3)$$

with L_R the radio luminosity, $F_{3\sigma}$ the flux density density sensitivity, and d_{sens} the resulting sensitivity distance. Then, the number of stars is

$$\#Stars = \left(\frac{f_{\text{sky}}}{4\pi} \right) \frac{4\pi n_{\text{obj}}}{3} \left(\frac{L_R}{4\pi F_{3\sigma}} \right)^{3/2} P(L_R) \quad (4)$$

where f_{sky} is the fraction of the sky visible from the ngVLA site, ≈ 10.3 steradian (Condon et al. 1998),

n_{obj} is the space density of the type of star, L_R the radio luminosity, $F_{3\sigma}$ the sensitivity threshold, and $P(L_R)$ the probability of the stellar object having that luminosity. We realize that the assumption of spherical geometry will break down at the scale of the Milky Way thick disk, or 1 kpc, but this treatment gives a simplified approach to the maximum distance detectable. Figure 5 plots the number of stars detectable with the ngVLA as a function of radio luminosity, using the radio luminosity distributions shown in Figure 4. Only luminosity ranges available from the data shown in Figure 4 are used, and inflections in the radio luminosity distribution show up as departures from the $\propto L_R^{3/2}$ trend of number of stars as a function of radio luminosity in Figure 5. The active binary systems have larger intrinsic radio luminosities than the M dwarf classes.

Figure 6 shows the number of stars detectable as a function of distance. Here the distance at which the trend for each type of star flattens indicates the distance at which the smallest radio luminosity present in Figure 4 is no longer detected. All stars are detectable at small distances, and the number scales as distance³. Eventually only the brighter stars are able to be detected at farther distances, so the rate of additional star counts decreases until no more stars would be detected at the largest distances. The calculation for M dwarfs used two different space density values as listed in Table 2.

TABLE 2
CATEGORIES OF RADIO-ACTIVE COOL STARS AND REFERENCES TO THEIR SPACE DENSITIES.

Category	Space Density stars pc ⁻³	Reference
active binaries	3.7×10^{-5}	Favata et al. (1995)
early-mid M dwarfs	0.08	Reid et al. (2007)
	0.05	Reid et al. (2008)
ultracool dwarfs	0.013	Reid et al. (2008)

Our approach for YSOs differed slightly. Since YSOs are found in clusters at discrete distances, for this population, we estimated the fraction of sources which would be detectable in a cluster similar to the ONC but placed further away. For these purposes we used the ngVLA’s continuum rms in one hour at 8 GHz to set the percent of sources detected for a 3σ detection. Figure 7 displays the result of this calculation, and demonstrates that 100% of the sources could be recovered in clusters at 2 kpc distance, sufficient to characterize many of the typical radio-emitting sources in star forming regions located in the nearest parts of the Sagittarius and Perseus arms of our galaxy.

3.2. Constraining Particle Distributions and Magnetic Fields in Magnetic Reconnection Flares

Radio observations provide a unique way to characterize the nature of the accelerated electron population near the star. This is important for understanding the radiation and particle environment in which close-in exoplanets are situated. An aspect of star-planet interactions which can be probed with radio observations is the magnetospheric interactions of a magnetized close-in planet with its host star. Similar to the

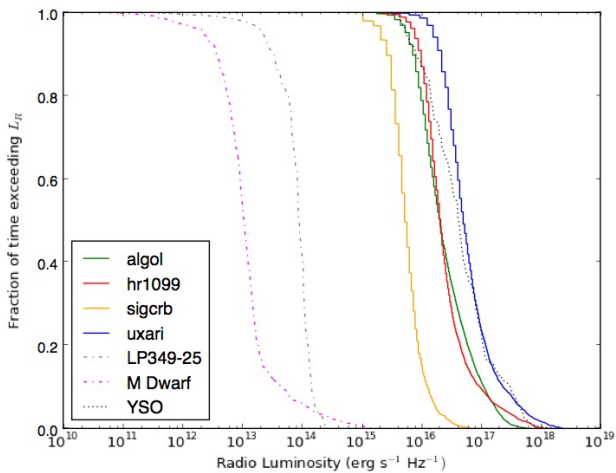


FIG. 4.— Cumulative distributions of 8 GHz cm radio luminosities for different categories of variable cool stellar objects: red, blue, yellow, and green histograms are active binary systems (Algal and RS CVn-type systems); the purple dashed histogram is the result of several multi-wavelength campaigns of the M dwarf flare star EV Lac (Osten et al. 2005, Osten et al. in prep.); grey red dotted histogram is the result of several monitoring observations of the ultracool dwarf LP349-25 (Ngoc et al. 2007, Osten et al. 2009); gray dotted histogram is the results of a deep centimeter-wavelength catalog of the Orion Nebula Cluster (Forbrich et al. 2016). Converting these to probability distributions enables a more realistic assessment of the likelihood of observing a given radio luminosity, and hence detectability of these types of radio sources, than averages or maximum luminosities.

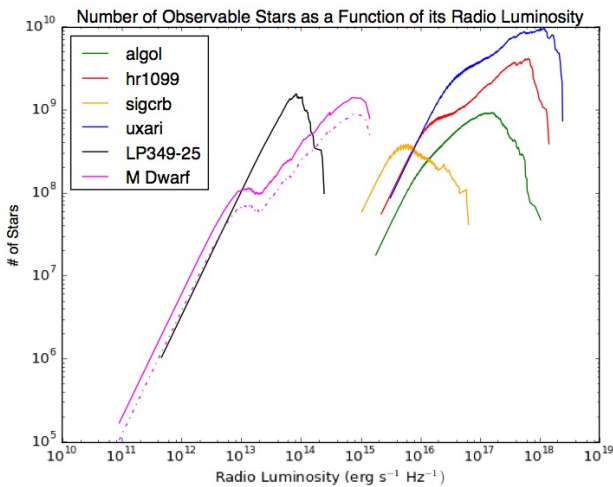


FIG. 5.— Number of stars detectable with the ngVLA as a function of radio luminosity, using the radio luminosity distributions shown in Fig. 4. A five minute integration, at a frequency of 10 GHz (check) is assumed.

idea that the proximity of two stellar magnetospheres due to close passage can cause periodic episodes of magnetic reconnection (as in Massi et al. 2006), recent results (Pillitteri et al. 2014) have suggested a triggering mechanism for regularly recurring stellar flares on stars hosting close-in exoplanets (hot Jupiters). For radio wavelength observations, the time-dependent response of radio emission reveals the changing nature of the magnetic field strength and number and distribution of accelerated particles. As stellar radio emis-

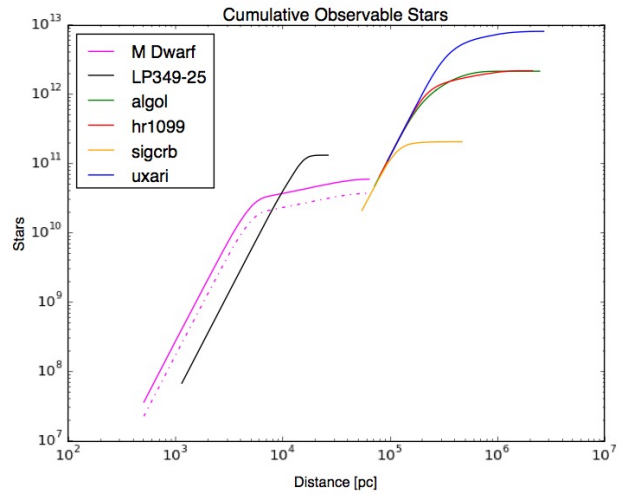


FIG. 6.— Cumulative number of stars observable as a function of distance.

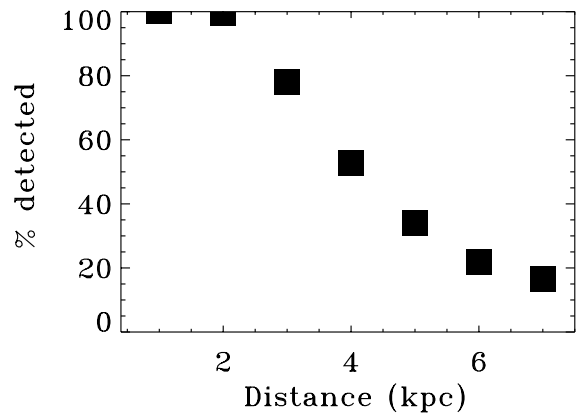


FIG. 7.— Percentage of the 478 radio sources detected in the deep exposure of the Orion Nebula Cluster reported by Forbrich et al. (2016), for clusters at various distances. Sensitivities appropriate to a one hour 8 GHz observation with the ngVLA are used.

sion typically has a peak frequency near 10 GHz, a wide bandwidth system spanning this range can probe the optically thick and thin conditions, diagnose the changing conditions during the course of a magnetic reconnection flare associated with close passage of an exoplanet, and deduce the nature of the accelerated particle population through measurements of spectral indices from confirmed optically thin emission. This would provide constraints on the accelerated particle population of close-in exoplanets unavailable from any other observational method; such a constraint is necessary to perform detailed modeling of the atmospheres of such exoplanets, due to the influence of accelerated particles in affecting the chemical reactions in terrestrial planet atmospheres (Jackman et al. 1990).

Smith et al. (2005) and Osten et al. (2016) laid out the basic framework for such a measurement, which requires multi-wavelength observations of the radio flare and its counterpart at higher energies. The uniqueness of the measurement lies in the difficulty in determining the characteristics of accelerated particles in nondegenerate environments in the cool half of the HR diagram. The usual technique for solar physicists is to deconvolve hard X-ray spectra exhibiting optically thin measurements of nonthermal bremsstrahlung emission to

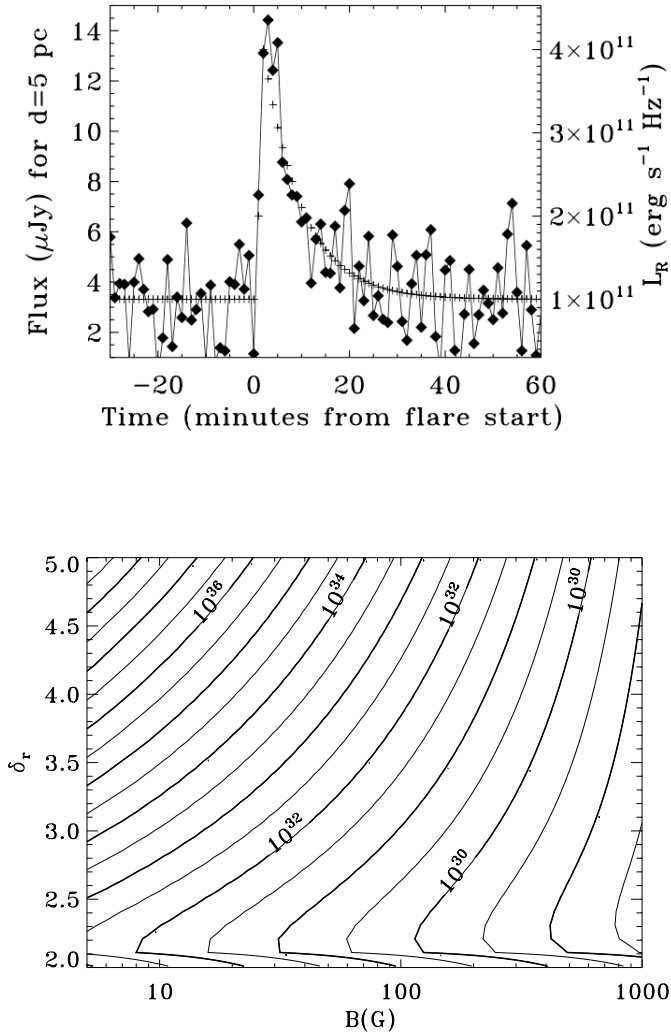


FIG. 8.— (top) Light curve of a short duration (lasting 5 minutes), small enhancement (factor of three increase above quiescence) flare on a nearby (5 pc) star. Right yaxis gives intrinsic radio luminosity, left axis gives the estimated radio flux density at 17 GHz. Noise is estimated in each 1 minute bin by offsetting the flux by a random number times the expected rms values. (bottom) Contour plot of δ_r , the index of accelerated particles, and B , the magnetic field strength in the radio-emitting source, for the radio flare seen above.

determine the power-law index of the accelerated electrons and source size. Because of astrophysical detector sensitivity coupled with typically hot thermal flaring plasma, this observational method has not yielded results in stellar cases. Radio constraints on accelerated particle characteristics are therefore the only measurement technique that will yield results for planet-hosting stars in the solar neighborhood.

The integrated radio flare energy provides a constraint on the accelerated particle kinetic energy, under the assumption of optically thin emission. The radio light curve provides constraints on both the index of the distribution of accelerated particles, as well as the magnetic field strength in the radio-emitting source. The contour plot of δ_r , the index of accelerated particles, versus the magnetic field strength in the radio-emitting source as a function of kinetic energy in the accelerated particles in a stellar superflare reported in Osten et al. (2016) was for an event with a peak radio

luminosity at 15 GHz of 5×10^{16} erg s $^{-1}$ Hz $^{-1}$. Based on Figure 5, there are numerous M dwarfs detectable with the ngVLA at the lower radio luminosity end, near 10^{11-12} erg s $^{-1}$ Hz $^{-1}$ for which similar analyses could be performed. Using the same methodology, we worked out the sensitivity to a radio flare with a peak flare enhancement of only 3 times this base level, for a flare lasting only 5 minutes total duration. Such an example is shown in the top part of Figure 8. These types of observations would be most sensitive to the nearest M dwarfs, in order to study time-variable emission over very short timescales (minutes). Quiescent radio luminosities as low as 10^{11} erg s $^{-1}$ Hz $^{-1}$ (at the limit of current detection capabilities; Osten et al. 2015) would be detectable in short integrations, allowing for study of small enhancement events only factors of a few larger. The kinetic energies probed here are moderate to large sized solar flares, and probe magnetic field strengths in the tens to hundreds of Gauss level.

A wide bandwidth system spanning the 10-20 GHz range can probe the optically thick and thin conditions, diagnose the changing conditions during the course of a magnetic reconnection flare associated with the close passage of an exoplanet, and deduce the nature of the accelerated particle population through measurements of spectral indices from confirmed optically thin emission. Operation of multiple subarrays would enable the frequency coverage available simultaneously to be significantly expanded. This would provide constraints on the accelerated particle population of close-in exoplanets unavailable from any other observational method; such a constraint is necessary to perform detailed modeling of the atmospheres of such exoplanets, due to the influence of accelerated particles in affecting the chemical reactions in terrestrial planet atmospheres.

4. SUMMARY

The influence that stars have on their near environments is a timely research topic now, and is expected only to grow in the future as exoplanet discoveries grow. While we expect that new discoveries in this area in the next decade will fill in some areas where we currently lack insight, there will remain gaps in our knowledge which can only be filled by a next generation sensitive radio telescope operating in the deka-GHz range.

5. REFERENCES

- Anglada-Escudé, G. et al. 2016 *Nature*, 536, 437
- Bower, G. et al. 2015 arXiv 1510.06432
- Condon, J. et al. 1998 *AJ* 115, 1693
- Crosley, M. K. et al. 2017 *ApJ* 845, 67
- Drake, S. A. et al. 1987 *AJ* 94, 1280
- Drake, J. et al. 2013 *ApJ* 764, 170
- Dressing, C. & Charbonneau, D. 2013 *ApJ* 767, 95
- Favata, F. et al. 1995 *A&A* 298, 482
- Fichtinger, B. et al. 2017 *A&A* 599, 127
- Forbrich, J. et al. 2016 *ApJ* 822, 93
- Garraffo, C. et al. 2016 *ApJ* 833, L4
- Garraffo, C. et al. 2017 *ApJ* 843, L33
- Heyner, D. et al. 2012 *ApJ* 750, 133
- Jackman, C. H. et al. 1990 *JGR* 95, 7417
- Johnstone, C. P. et al. 2015 *A&A* 577, 28
- Lovell, R. et al. 2008 *MNRAS* 389, 1233
- Massi, M. et al. 2006 *A&A* 453, 959

- Ngoc, P. et al. 2007 ApJ 658, 553
Osten, R. A. & Bastian, T. 2006 ApJ 637, 1016
Osten, R. A. & Bastian, T. 2008 ApJ 674, 1078
Osten, R. A. et al. 2005 ApJ 621, 398
Osten, R. A. et al. 2009 ApJ 700, 1750
Osten, R. A. et al. 2016 ApJ 832, 174
Osten, R. A. & Wolk, S. J. 2015 ApJ 809, 79
Osten, R. A. & Wolk, S. J. 2017 IAUS 328, 243
Panagia, N. & Felli, M. 1975 A&A 39, 1
Pillitteri, I. et al. 2014, ApJ 785, 145
Reid, I. N. et al. 2007AJ 133, 2825
Reid, I. N. et al. 2008 AJ 136, 1290
Richards, M. et al. 2003 ApJS 147, 337
Segura, A. et al. 2010 AsBio 10, 751
Smith, K. et al. 2005 A&A 436, 241
Tian, F. et al. 2014 E&PSL 385, 22
Venot, O. et al. 2016 ApJ 830, 77
Vidotto, A. et al. 2015 MNRAS 449, 4117
Wargelin, B. J. & Drake, J. 2001 ApJ 546, L57
Wood, B. E. et al. 2004 AdSpR 34, 66
Wood, B. E. et al. 2014 ApJ 781, L33
Wright, A. E. & Barlow, M. J. 1975 MNRAS 170, 41

The National Radio Astronomy Observatory and Green Bank Observatory are facilities of the U.S. National Science Foundation operated under cooperative agreement by Associated Universities, Inc. This work was supported by awards AST-2034328 (MSIP Prototype Antenna) and AST-2334267 (ngVLA Design Activities); NRAO related activities are funded under award AST-1647378 (NRAO Operations/Development).

